Numerical studies of ion focusing behind macroscopic obstacles in a supersonic plasma flow

W. J. Miloch* and J. Trulsen
University of Oslo, Institute of Theoretical Astrophysics, Box 1029 Blindern, N-0315 Oslo, Norway

H. L. Pécseli
Department of Physics, University of Oslo, Box 1048 Blindern, N-0316 Oslo, Norway

(Received 11 December 2007; revised manuscript received 22 March 2008; published 29 May 2008)

We study the potential and plasma density variations around a solid object in a plasma flow, emphasizing supersonic flows. These objects can be dust grains, for instance. Conducting as well as insulating materials are considered. In a streaming plasma, a dust grain develops an electric dipole moment, which varies systematically with the relative plasma flow. The strength and direction of this dipole moment depends critically on the material. The net charge together with the electric dipole associated with the dust grains gives rise to electric fields, which affects the trajectories of nearby charged particles. The perturbation of ion orbits in streaming plasmas can give rise to a focusing of ions in the wake region facing away from the plasma flow. We study the parameter dependence of this ion focus. Our simulations are carried out in two spatial dimensions by a particle-in-cell code, treating ions and electrons as individual particles.

DOI: 10.1103/PhysRevE.77.056408 PACS number(s): 52.27.Lw, 52.65.Rr

I. INTRODUCTION

The potential distributions surrounding solid objects, such as dust grains, in plasmas depend critically on the plasma conditions [1]. In thermal equilibrium we find the standard electrostatic Debye shielding. When the grains are exposed to a streaming plasma the conditions can change significantly. One conspicuous new feature that has been noted is manifested by a focusing of ions in the region behind the grain, in the wake facing away from the flow direction [2]. The ion focusing is shown to be the most likely candidate to explain the vertical alignment of macroscopic dust grains that are levitated in the sheath region of discharges used in experiments [3–5]. This nonreciprocal vertical interaction between dust grains can, under certain conditions, be the source for an oscillatory instability, which leads to a phase transition of crystalline dust structures [6]. The other approach, which concerns the linear response of a collisionless plasma with the ions flowing around a pointlike dust grain, shows an oscillatory wake potential behind the dust [7–11]. This analysis can be extended to include dust with a finite size and anisotropic charge distribution on its surface. It is shown theoretically that the finite size becomes important for dust radii comparable to the Debye length, i.e., $a \approx \lambda_D$ [12]. The electric dipole moment will also have a strong influence on the strength and position of potential extrema [12,13]. The test charge approach used for different electron to ion temperature ratios, shows that the perturbations in the potential are stronger for larger ratios [14]. Vertical alignment of dust grains is generally accepted to be caused by ion focusing, while the ion drag force [15] only modifies this effect [16,17].

The full problem is in reality far more complicated than that considered in theoretical approaches. The linear theory will not hold for highly charged dust grains, when ion trajectories are highly distorted and some of the ions are trapped. The standard analysis does not include the wake in the plasma density, which develops due to the plasma flow around the object of finite size. (We refer to the density wake as the region in the shadow of the object, where the electron and ion densities are reduced by more than approximately 50%). Therefore, for the more complete description one could consider numerical simulations, which can address nonlinear problems in a consistent way.

Previous numerical works revealed the existence of an ion focusing region behind an object or a dust grain and studied this phenomenon for some selected cases and parameters [18–21]. The ion focusing was also observed in other numerical simulations for charging of individual dust grains or objects in plasmas, where it was attributed to orbital effects in the vicinity of the object [15,22,23]. Many numerical models, which were used in previous studies of the ion focusing effect, were not fully self-consistent concerning the charging of the object. The dust grain was represented either as an object of finite size that was biased at an arbitrarily chosen potential [18], or by a pointlike grain with a fixed charge [20,21]. Thus, these simulations could only mimic conducting objects with some uncertainty for the floating potential. However, once the finite size effect of the object becomes important, the disturbance in the plasma induces an electric dipole moment on the conducting object. This is observed or mentioned already for moderate radii of the object [23,24]. The charge distribution becomes even more conspicuous for insulating objects. Here, it was shown that due to the flow, an electric dipole moment will develop, which strongly influences the surrounding plasma [23,25–27]. Since insulating dust grains are often used in laboratory experiments of dusty plasmas, one should consider insulating dust grains also in simulations. Self-consistent simulations should also include the stochastic nature of the dust charging process in plasmas. Therefore, the challenge for numerical simulations is to mimic the entire charging process. Such a self-consistent approach was proposed in particle-in-cell (PIC) simulations for small conducting objects (with the

*w.j.miloch@astro.uio.no

charge being uniformly distributed on the surface) [17]. The issue was also addressed in molecular dynamics simulations for small conducting grains [19,28,29]. However, due to the high computational cost of the molecular dynamics simulations, the entire charging process could not be resolved there. The authors had to specify the initial charge on the dust, and could run the code only for time intervals of ~0.5 in units of ω_{pi}^{-1}. For the same reason only a rather small volume close to the dust grain could be simulated.

In the present paper we present parametric studies of ion focusing with the PIC code in two spatial dimensions. We demonstrate the ion focusing for insulating, or alternatively conducting, objects of different sizes and shapes, and study the effect for different electron to ion temperature ratios γ and for different ion flow velocities v_d. We simulate the entire charging process for a single object in a collisionless plasma. We treat electrons and ions as individual particles, and are thus able to consider the stochastic nature of the whole charging process within the limitations inherent in the PIC method.

We should note here that the basic physical features are the same for two and three dimensional systems, and that our results can be directly applied, for instance, to elongated objects placed perpendicular to the plasma flow. Ion focusing will be stronger for the three dimensional case [18].

II. NUMERICAL CODE

The numerical analysis is carried out by a PIC code. The basic features of the program are standard, and need not be discussed in detail here [30]. We mention just briefly some specific features. Our code is two dimensional, implying for instance, that circles represent a stick with a circular cross section, where the axis is perpendicular to the simulation plane. Other codes [15,22] impose cylindrical symmetries, and can simulate the plasma flow around a sphere in a formally two dimensional representation. We treat electrons and ions as individual particles, where some other codes simplify the problem by considering the electrons as a locally isothermal and Boltzmann distributed fluid [22,31]. By this latter procedure only the ion time scale needs to be considered, but this simplification is obtained at the expense of a nonlinear Poisson equation. Such a model does not account for electron absorption on the surface. In our code, a typical time step is $0.01/\omega_{pe}$ to advance the particles on a fixed square grid, using a standard leapfrog scheme. We do not assume quasineutrality during the simulations, but we monitor the overall neutrality of the system. Poisson's equation is here solved by a standard iterative Gauss-Seidel method. Ion drag forces [15] are not considered in the present work.

The problem is analyzed with two boundary conditions for Poisson's equation, one at the outer boundaries, where ions and electrons are injected according to *a priori* chosen velocity distributions. Particles are initially also distributed internally in the simulation area (except for regions occupied by the dust), according to selected velocity distributions. Therefore we expect initial transients in the system to occur. Particles can leave freely across any outer boundary, while particles are injected at all boundaries, according to the selected velocity distribution function. The streaming velocity is parallel to the positive x axis, with a shifted Maxwellian distribution. Ions and electrons stream with the same average velocity. Since the flow velocity of our interest is larger than the ion thermal velocity and much lower than the electron thermal velocity, it suffices to describe it in terms of the ion flow velocity v_d.

The second inner boundary defines the nature of the individual dust grain. For perfect insulators, we assume that a charged particle hitting the surface remains at that position for all later times, contributing to the total electric field distribution. For perfect conductors, the electrostatic potential is the same for all positions at this boundary, and the electric field vanishes inside. The dust grain is assumed to be rigid and massive, i.e., it retains its initial shape and remains immobile for the duration of the simulation. Our simulations with conducting materials have many properties in common with related studies of Langmuir probe performance in collisionless plasmas [32,33].

The geometry of our problem is different from the one considered by others [15,22], so a detailed comparison is difficult. We note, however, that the Mach cone, which is expected on theoretical grounds, is more clearly developed in our simulations. While codes imposing symmetry in the system limit the possible shapes of the simulated objects, our code allows for studies of complex shaped objects, as for example, elongated objects or plane Langmuir probes. In particular, our code has been verified by operating it in a "Langmuir probe mode," where a fixed potential on the inner boundary is imposed externally. We here reproduced probe characteristics for standard conditions, as well as for more complicated conditions with plane probes embedded in plasmas with ion beams [34–36]. Moreover, the code allows many dust grains to be distributed inside the simulation area, but for the present analysis we limit the case to only one. More details concerning our code, with a discussion of the ion to electron mass ratios and the grid spacing, have been given elsewhere [23].

For the present study, the code is operated with fixed potentials at all outer boundaries. We use a 200×200 grid resolution for a simulation area of 50×50 in units of λ_{De}^2. With a grid spacing of 0.25 in units of λ_{De}, we can resolve also the Debye length. Our results are presented in normalized units, but when initiating the code we introduce physically relevant parameters, with the exception of the electron to ion mass ratio. The total Debye length ($\lambda_D^{-2}=\lambda_{De}^{-2}+\lambda_{Di}^{-2}$, with λ_{Di} denoting the ion Debye length) varies in the present study with the ion temperature, and is in the range $\lambda_D\in(1.0-4.1)\times10^{-5}$ m. The electron temperature and the electron Debye length are fixed at $T_e=0.18$ eV and $\lambda_{De}=10^{-4}$ m, respectively. For completely static phenomena the correct length for the normalizations of the spatial coordinates would be the total Debye length λ_D. For the large streaming velocities relevant in this work, the ions do not contribute effectively to the shielding of the dust, so we use λ_{De} to normalize the results. With time resolution of $\Delta t=0.012$ in units of ω_{pe}^{-1}, we avoid that plasma particles move more than one grid cell within one time step. We use an ion to electron mass ratio of 120, which is large enough to give credibility to our results

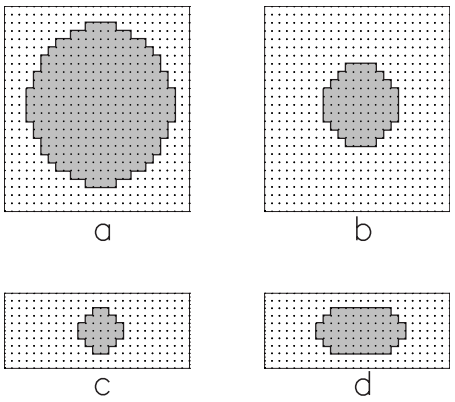

FIG. 1. Illustration of dust shapes considered in the present study. The small dots show the numerical grid, shapes (a)–(c) are as close to a circle as possible with the given grid resolution, with radius: (a) $a=2.5\lambda_{De}$, (b) $a=1.25\lambda_{De}$, and (c) $a=0.625\lambda_{De}$. Shape (d) is an elongated grain with eccentricity $\epsilon=\sqrt{3}/2$, with the major axis $a=1.25\lambda_{De}$.

[23], and run the simulations with the following electron to ion temperature ratios: $\gamma=\{5,10,20,40,60,80,100\}$.

We analyze obstacles with four different shapes or sizes. Three of the obstacles represent a shape as close to being circular as possible for the dust implementation on the square mesh in our numerical code [Figs. 1(a)–1(c)]. Their radii are $a=2.5$, 1.25, and 0.75 in units of λ_{De}. As an example of an obstacle with a different shape we have an elongated object with eccentricity $\epsilon=\sqrt{3}/2$ [Fig. 1(d)]. The obstacles are either perfectly conducting or perfectly insulating, and are placed well inside the simulation area.

The plasma density is $n=10^{10}$ m^{-2}, which we simulate using approximately 2.5×10^5 simulation particles, for both electrons and singly charged ions. This density corresponds to $n=10^{15}$ m^{-3} in the three dimensional system, and is typical for glow or rf discharge plasmas. The electron temperature is 0.18 eV. Such a temperature is found in the plasma sheath in rf discharges that are commonly used for dusty plasma experiments [37]. The electron to ion temperature ratio in rf discharges may be as large as $\gamma=100$ in the bulk plasma [4].

We typically run the code until it reaches steady state conditions, typically after three ion plasma periods τ_i for subsonic flows. Since the ion flow acts as an energy input to the system, we are particularly interested in the asymptotic charging characteristics of dust grains for fast ion flows. For fast flows we find asymptotic conditions after approximately nine ion plasma periods. In order to have statistically satisfactory results, we run our code typically for 12 ion plasma periods.

III. NUMERICAL RESULTS

We observe focusing of ions in the wake behind the dust grain in the presence of ion drifts. Vector plots of the average ion velocity reveal that the ion trajectories are bent toward the focal region behind the dust grain (see Fig. 2). The bending is stronger for insulating grains. This is shown in the

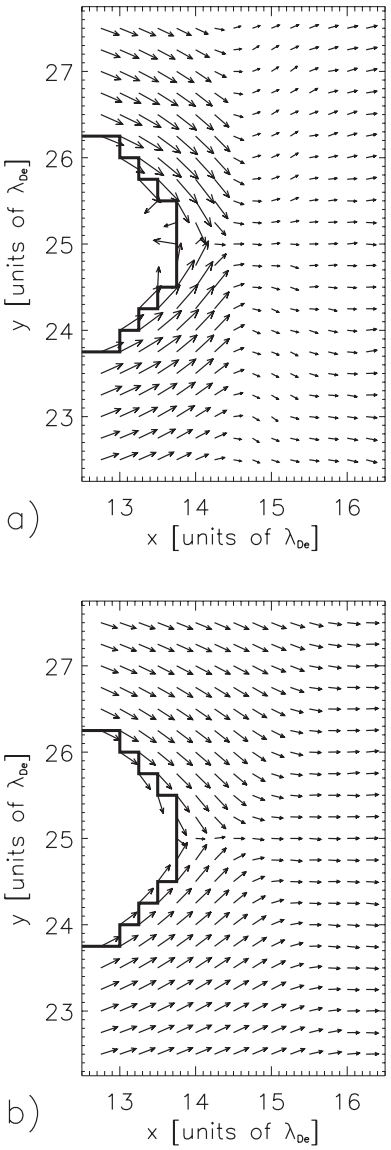

FIG. 2. Averaged ion velocity around an insulating (a) and conducting (b) dust grain with a shape given by Fig. 1(b). The arrows show the average ion velocity per simulation cell (averaged over 1.5 ion plasma periods τ_i). The electron to ion temperature ratio is $\gamma=40$, and ion drift velocity $v_d=1.5$ in units of C_s. The ion density has a spatial variation, which gives $\nabla\cdot(n_i\mathbf{u_i})=0$, consistent with the continuity equation for stationary conditions.

$x-v$ phase space plots for the ions in Fig. 3. The phase space plots refer to ions located within a narrow slice of the simulation area. The width of the slice is equal (width 2.5 in units of λ_{De}) to the diameter of the dust. The slice is centered on the dust and oriented along the x axis. The ion flow is in the positive x direction, and the center of the dust grain is located at $x=12.5$ in units of λ_{De}. In the wake behind the insulating dust grain, there is a significant number of ions that have the velocity component v_x parallel to the ion drift ranging from zero to approximately the average ion drift velocity v_d. The strong bending of the ion trajectories behind the dust is most visible in the velocity component v_y, perpendicular to the drift. Here, the ions that are closest to the dust are nearly grazing its surface and have speeds close to

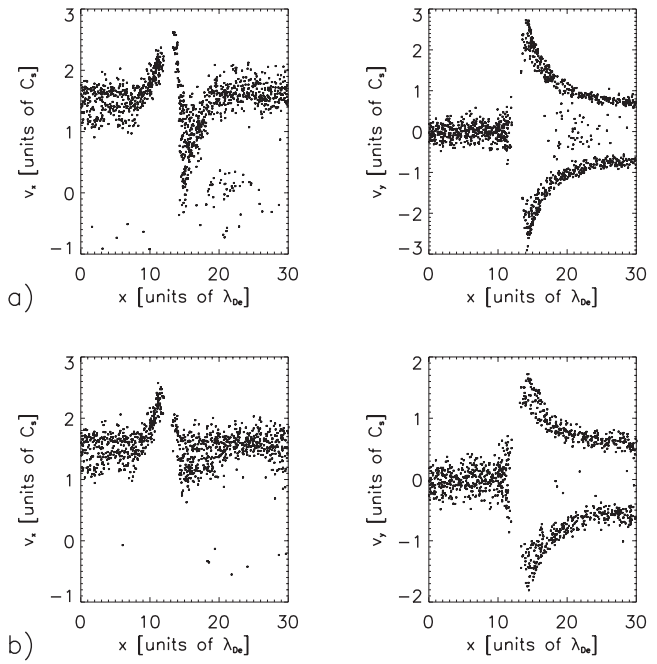

FIG. 3. The $x-v_x$ and $x-v_y$ phase space plots for a plasma with ion drift velocity $v_d=1.5$ in units of C_s for perfectly insulating (a) and perfectly conducting (b) dust grains with the shape given by Fig. 1(b). The plots correspond to an average over a narrow slice of the simulation box along the x axis. The slice has a width of $2.5\lambda_{De}$ and goes through the center of the dust. The center of the grain is at $x=12.5\lambda_{De}$, and its radius is $1.25\lambda_{De}$. The electron to ion temperature ratio here is $\gamma=40$.

the ion drift velocity. These ions correspond to the peak velocities observed just behind the dust grain in the $x-v_y$ plot.

For the conducting dust the corresponding peak velocities are smaller than for the insulator (see Fig. 3). There are also much fewer particles with small parallel velocity components v_x. Thus, for the conducting dust, the ion focusing is weaker and the focal region is wider. Far from the object both cases appear similar. The velocity component v_y perpendicular to the ion flow is still significant, with a pronounced symmetry with respect to the x axis in the $x-v_y$ plot.

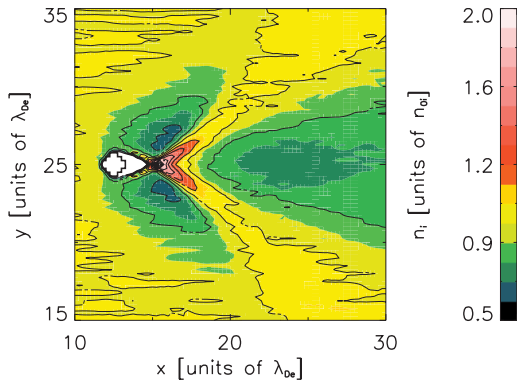

FIG. 4. (Color) Averaged ion density n_i for a plasma with ion flow velocity $v_d=2.5$ in units of C_s for an insulating dust with the shape given by Fig. 1(c). The densities are averaged over 1.5 τ_i at the end of the simulations. The electron to ion temperature ratio is $\gamma=80$. The white region represents density ratios $n_i/n_{i0}<0.5$. The ion drift is in positive x direction.

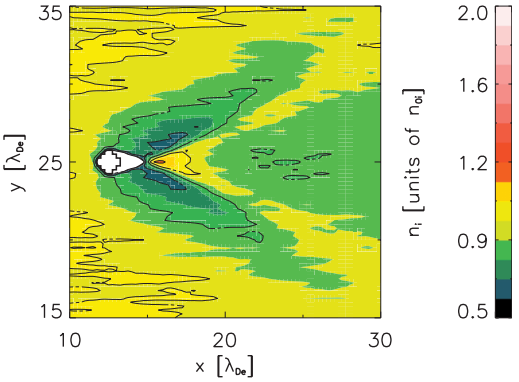

FIG. 5. (Color) Averaged ion density n_i for a plasma with ion flow velocity $v_d=2.5C_s$ for a conducting dust with the shape given by Fig. 1(c). The densities are averaged over $1.5\tau_i$ at the end of the simulations. The electron to ion temperature ratio is $\gamma=80$.

To substantiate the foregoing discussion we present plots of time averaged ion densities for insulating as well as conducting objects. The ion focusing is strong behind the insulating dust, where we find a distinct peak in the ion density (see Fig. 4). This peak in density is more pronounced than the corresponding one behind the conducting dust, as shown in Fig. 5. For the latter case, we often notice an oscillatory pattern in ion density along the ion flow (see Fig. 6). For the insulator, such a pattern is probably dominated by the strong ion focusing. For both insulating and conducting grains we observe Mach cones in the ion density, for Mach numbers $M>1$, consistent with previous simulations [23].

To quantify our results, we introduce a number of parameters defined in Fig. 7. We refer to the total ion focusing strength n_f as the maximum peak in the ion density with respect to the undisturbed ion density. Similarly, we introduce the relative ion focusing strength n_r. The focusing strengths n_f and n_r depend on both the ion drift v_d and the electron to ion temperature ratio γ. There is little focusing for a subsonic flow. For increasing supersonic flows the focusing strengths n_f and n_r have a maximum and then decrease again. Grains with a radius larger than λ_{De} have the maximum around $M=2$. For grains with $a<\lambda_{De}$, the maxi-

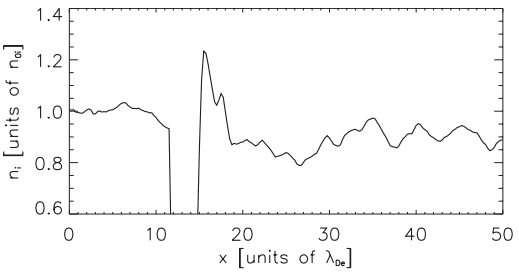

FIG. 6. Averaged ion density n_i for a plasma with ion flow velocity $v_d=2.5C_s$ for a conducting dust with the shape given by Fig. 1(c). The densites are averaged over $1.5\tau_i$ at the end of the simulations. The electron to ion temperature ratio is $\gamma=80$. The figure shows the density along the x axis, at $y=25$ in units of λ_{De}.

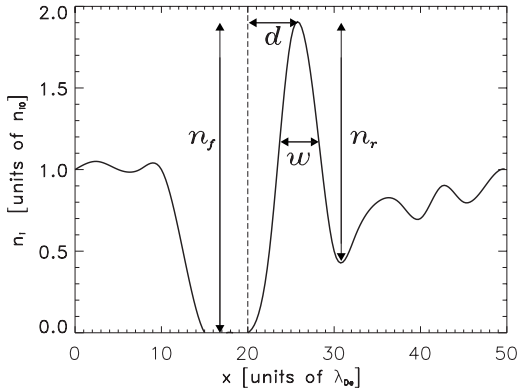

FIG. 7. Definition of parameters used for quantifying the simulation results. The vertical dashed line shows the rear edge of the dust grain.

mum occurs at $M=1.5$. The extremum is more conspicuous for these grains than for larger grains (see Fig. 8), with the corresponding decrease for larger Mach numbers also being more pronounced. The irregularities of the curves are a measure of the uncertainities on the estimates here and in the following. The total focusing strength n_f increases systematically with γ. For $\gamma=5$ the maxima of the total focusing strength are weak and reach $n_f \approx n_i$, while for $\gamma=100$ the maxima are much more pronounced. For smaller grains $a<\lambda_{De}$, the total focusing strength reaches up to $n_f \approx 3n_i$ (see Fig. 9).

We do not observe ion focusing behind conducting grains with radii $a \geq 2.5\lambda_{De}$. For medium and small size conducting grains, the total focusing strength reaches a saturation level at approximately $n_f \approx n_i$ already for $M=1$. This saturation level depends only slightly on γ. We studied ion focusing behind conducting dust grains with shape given by Fig. 1(c) as a function of ion drift velocity for different electron to ion temperature ratios γ. Here the ion focusing is strongest for $M=1$ and for high γ, which is revealed by the maximum in the relative focusing strength n_r. The focusing strength is approximately half the corresponding value observed for insulators.

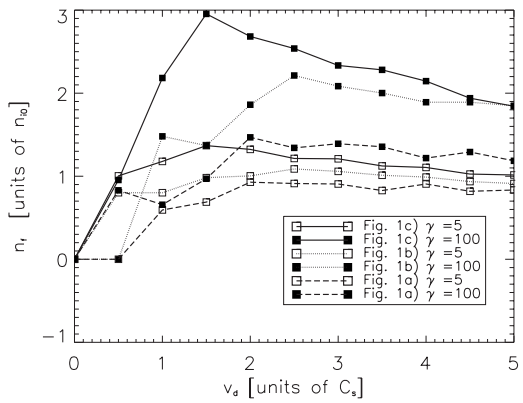

FIG. 8. The total ion focusing strength n_f behind insulating dust grains of different size as a function of ion drift velocity. For convenience we plot results only for electron to ion temperature ratios $\gamma=5$ and $\gamma=100$.

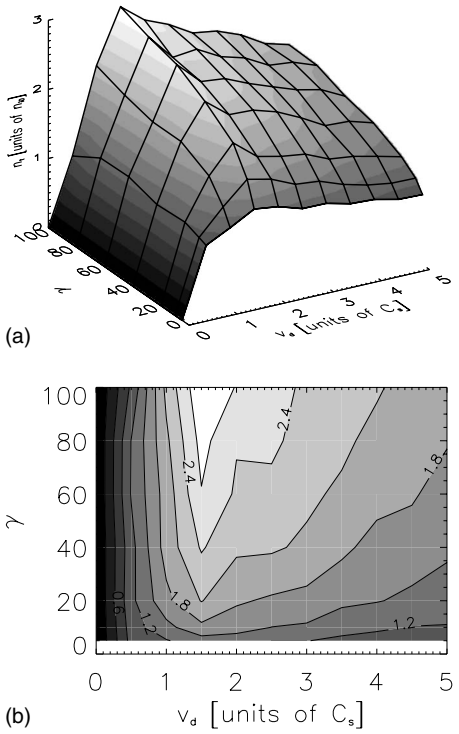

FIG. 9. The total ion focusing strength n_f behind insulating dust grains with shape given by Fig. 1(c) as a function of ion drift velocity for different electron to ion temperature ratios γ.

A high relative focusing strength n_r is characteristic for highly concentrated focal regions, i.e., small full width at half height w, as defined in Fig. 7. For higher Mach numbers we observe a decrease in the relative focusing strength n_r for both conducting and insulating grains (Fig. 10). For insulators this decrease is observed together with the elongation of the focal region w. Such an elongation of the focal region is not so pronounced behind conductors, due to smaller total focusing strength n_f and the oscillatory component, which we already mentioned.

Another interesting parameter is the distance d between the maximum of the focusing and the surface of the dust (see

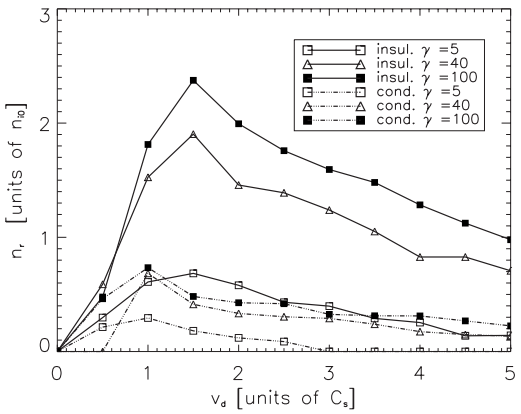

FIG. 10. The relative ion focusing strength n_r behind insulating and conducting dust grains with shape given by Fig. 1(c) as a function of ion drift velocity for different electron to ion temperature ratios γ.

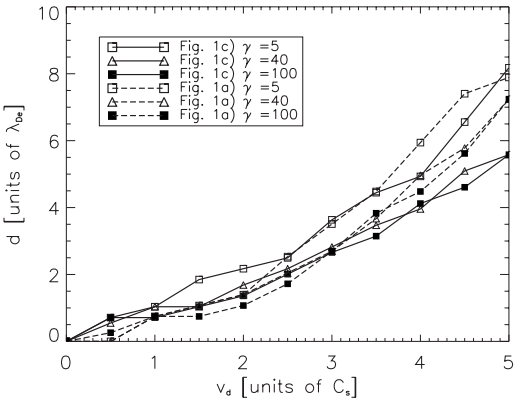

FIG. 11. The distance d between the rear of the dust grain and the peak for ion focusing behind insulating dust grains with shapes given by Fig. 1(a) and by Fig. 1(c) as a function of ion drift velocity for different electron to ion temperature ratios γ.

Fig. 7). For the given range of velocities v_d, the value of d is between $1-9\lambda_{De}$ for insulators. There is no apparent dependence on the radius of the dust (see Fig. 11). We find that d depends slightly on the parameter γ, being smaller for larger temperature ratios. We do not find that d scales as λ_{Di} or λ_D, which confirms that supersonic ions do not effectively contribute to the shielding of the dust grain [10]. The slight dependence on γ reflects the mobility of ions in the direction perpendicular to the flow, i.e., cold ions nearly grazing the surface will be focused, while parts of the corresponding warmer ions will be lost on the dust surface. This suggests that the position of the maximum is an orbital effect related to the wake formation behind the dust. For conductors, we find the corresponding values of d to increase by approximately a scaling factor 1.5–2 (see Fig. 12). As compared to Fig. 11, the variations in d have a larger scatter when γ is varied and when the size of the dust grain is changed. Apart from the difference in scaling factor mentioned before, we find that the d-parameter variations in Figs. 11 and 12 are similar.

For a model calculation of a cylindrical object by using standard orbit theory [38], the cylindrical symmetry will imply a typical ion deflection distance being between zero and the sheath thickness, which is of the order of λ_{De}. In reality the wake behind the dust is breaking the cylindrical symmetry, and the focusing distance is enhanced, in particular, for conducting objects.

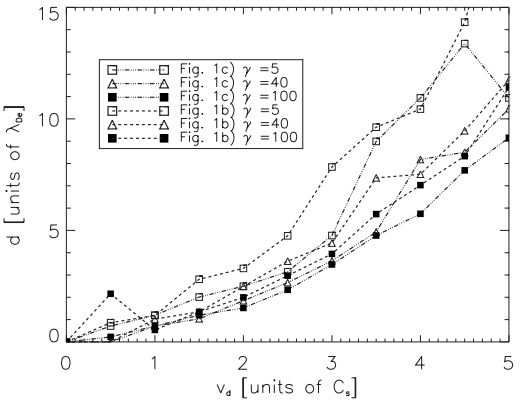

FIG. 12. The distance d between the rear of the dust grain and the peak for ion focusing behind conducting dust grains with shapes given by Fig. 1(b) and by Fig. 1(c) as a function of ion drift velocity for different electron to ion temperature ratios γ.

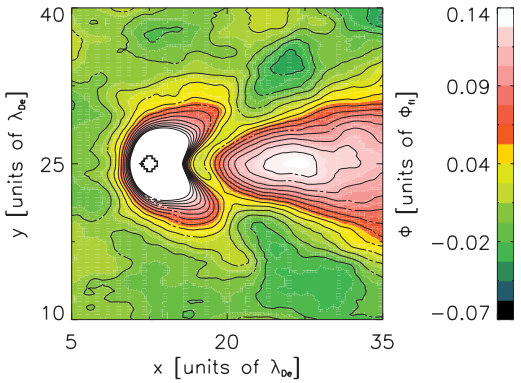

FIG. 13. (Color) Potential variation for a plasma with ion flow velocity $v_d=2.5$ in units of C_s around an insulating dust with the shape given by Fig. 1(c). The potentials are averaged over $1.5\tau_i$ at the end of the simulations. The electron to ion temperature ratio is $\gamma=100$. Only potentials close to the plasma potential $\Phi_{pl}=0$ are colored. Potential is normalized with the floating potential $\Phi_{fl}<0$ consistent with our previous results [23]. The ion drift is in the positive x direction.

We observe a weak but stationary enhancement in the potential, with the maximum corresponding to the ion focal region (see Figs. 13 and 14). The potential enhancement is stronger for insulating grains. In particular, we find here the strongest potential enhancement directly behind the grain, and two weaker slopes on the sides, further down from the ion focus, that correspond to ions streaming out from the focal region. For both insulators and conductors, we find fluctuating potentials in the wake of the dust, but these fluctuations diminish upon averaging. The remaining dominant feature is the enhanced potential in the focal region. For supersonic ion drifts we observe a Mach cone in the poten-

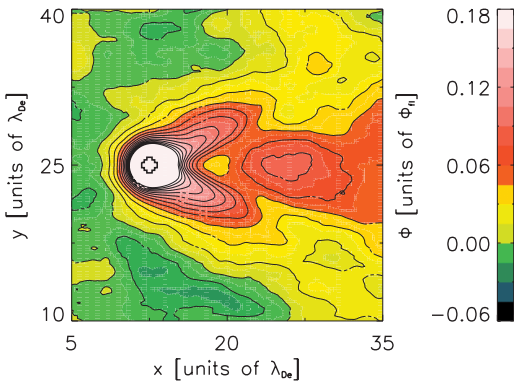

FIG. 14. (Color) Potential variation for a plasma with ion flow velocity $v_d=2.5$ in units of C_s around a conducting dust with the shape given by Fig. 1(c). The potentials are averaged over $1.5\tau_i$ at the end of the simulations. The electron to ion temperature ratio is $\gamma=100$. Only potentials close to the plasma potential $\Phi_{pl}=0$ are colored. Potential is also normalized here with the floating potential $\Phi_{fl}<0$ consistent with our previous results [23].

tial. The Mach cone is more pronounced behind insulators. For this case, we observe also a second cone with the source directly behind the grain. The spatial extent of the first one, which is due to the supersonic flow around the dust grain, is reduced by the ions streaming out from the focal region.

IV. DISCUSSION AND CONCLUSIONS

The charging of dust grains in streaming plasmas have been studied by numerical methods using a PIC code. Particular attention was given to conditions where ion focusing could be observed at supersonic plasma flows. In previous studies, we also analyzed solid obstacles placed in streaming plasmas. In that analysis we used relatively modest temperature ratios $T_e/T_i=5$ and found that ion focusing was only marginally observed for insulators and not at all for conductors [23]. For this reason, we use enhanced temperature ratios in the present analysis, keeping in mind that a ratio γ as large as 100 may have physical or practical relevance [4].

For insulators, the electric fields in the vicinity of the dust grain will be enhanced relative to the corresponding case of a conducting grain. The ion trajectories are strongly deflected. For a conductor, on the other hand, the short-circuiting effect will reduce the strength of the corresponding local electric fields, with the corresponding ion trajectories being less perturbed. This feature will be the same for circular and elongated grains. The electron pressure gradient at the density depletion associated with the wake gives rise to ambipolar electric fields, which will then deflect the ions to form an ion focus at a larger distance from the grain surface. The width of the focusing region w in Fig. 7 is consequently also larger. For large size conductors, we expect that it is just as much the wake depletion that controls the ion focusing, contrary to an insulator, where the dominant effect is due to the charge and dipole moment associated with the dust grain itself. Consistently with this observation, we expect that the difference between insulators and conductors should diminish as we reduce the size of the dust, thereby reducing the wake density depletion. Consequently, the distance d should diminish with the dust size for conductors but be only slightly affected for insulators: we indeed observe these features.

Taking an elongated conducting dust [Fig. 1(d)], with its longer axis being parallel to the ion drift, we find that for small drift velocities many ions get deflected as soon as they come close to the dust, and become absorbed at the surface. This absorption will become relatively less important as the flow velocity is increased. We observe the consequences of this feature as an absence of a local maximum of the focusing strength n_f around $M\approx 1$ for elongated grains, while this local maximum can be clearly observed for circular grains of similar transverse diameter.

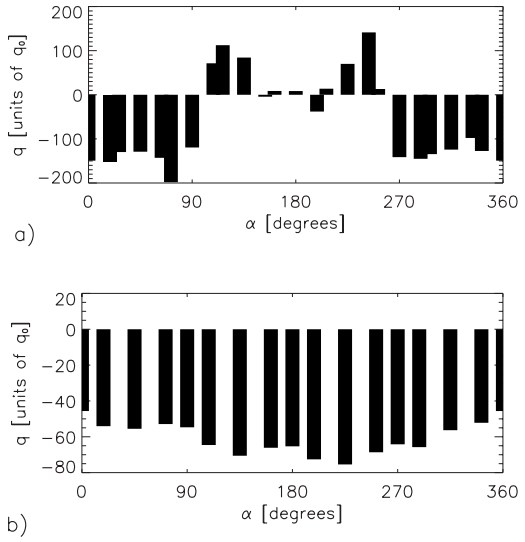

FIG. 15. The charge distribution q on the insulating (a) and conducting (b) dust grains given by Fig. 1(c) in a flowing plasma with $v_d=2.5$ in units of C_s for the electron to ion temperature ratio $\gamma=80$. The charge is normalized by the two dimensional elementary charge $q_0=e[n_{i0}]^{1/2}$. The abscissa corresponds to the angle between the half-line going from the center of the grain in the direction of the flow and the line connecting the center and the surface of the dust grain, so that $\alpha=180°$ corresponds to the point directly facing the plasma flow.

In order to illustrate the charge distribution on the surface of the dust particles, we show results for a circular particle in Fig. 15. The abscissa on both figures gives the angle between the half-line going from the center of the grain in the direction of the flow and the line connecting the center and the surface of the dust grain, so that $\alpha=180°$ corresponds to the point directly facing the plasma flow. The distribution of the bars appears irregular because we have to represent the circle on a square mesh. We note a pronounced difference between insulators and conductors, predominantly in the region facing the plasma flow. The asymmetry in the charge distribution is due to the statistical scatter in the charges on the surface elements.

It has been shown before [23] that a significant electric dipole moment develops on the insulating dust in the presence of ion drifts. We do not find any significant correlation between the ion focusing strength and the total electric dipole moment on the dust. We do, however, find good correlation between the total charge on the dust and the ion focusing strength for insulators, in particular. In Table I we present

TABLE I. The coefficient p_1 for the linear least-squares fit $n_f=p_1q_{tot}+p_2$ for insulating and conducting dust grains with the shape given by Fig. 1(c). Only supersonic velocities were considered. The relative uncertainty $\delta p_1/p_1$ is for both cases of the order of 10% for $\gamma\geq 10$ and 30% for $\gamma=5$.

γ	5	10	20	40	60	80	100
p_1, insulator	4.1	9.0	12.9	19.8	27.0	27.7	38.3
p_1, conductor	6.1	1.1	1.5	2.3	2.5	2.7	1.8

the results of a linear least-squares fit for $n_f = p_1 q_{tot} + p_2$. We considered both insulating and conducting grains. The linear fit is done for supersonic ion velocities for dust grains with shape given by Fig. 1(c). By varying the flow velocity we vary the charge on the dust, i.e., the changes in the dust charge originate from the corresponding changes in the ion flow. The total charge q_{tot} was normalized with

$$Q_0 = -\pi\epsilon_0 \frac{\kappa T_e}{e}\left[\ln\left(\frac{M}{2\pi m}\right)+1\right]\frac{R}{\lambda_D}\frac{K_1(R/\lambda_D)}{K_0(R/\lambda_D)}, \qquad (1)$$

where R is a radius of the grain, and K_0 and K_1 are modified Bessel functions [23]. Note that Q_0 in Eq. (1) changes with γ due to the presence of λ_D as defined before. In general, the ion focusing strength is directly proportional to the total charge on the dust. For the insulators, the proportionality constant p_1 depends on the temperature ratio γ being larger for increasing γ. For small T_i (and thus for large γ), the ion focusing region will be more concentrated, because of the reduced spread in ion thermal motion.

The proportionality constant p_1 is consistently smaller for larger objects (these results are not shown here). This is due to the lower local charge density on the shadow side for this case. For macroscopic insulating objects, most of the total charge will be localized on the shadow side. This will result in a complex potential distribution, which will lead to particularly strong electric fields. For conductors the proportionality constant p_1 is approximately one order of magnitude lower than for insulators. There is also no clear dependence on the temperature ratio γ in this case. This again confirms that the charge distribution on the equipotential surface cancels strong electric fields, and that in this case the focusing is governed mainly by the ambipolar diffusion. We conclude that the macroscopic charge distribution on the insulating surface is crucial for the ion focusing. Here, the anisotropy in the dust charging process is important, but the focusing strength n_f does not depend on the magnitude of the resulting electric dipole moment of the whole grain. A representation using only a point charge and an electric dipole is inadequate for explaining our observations. The range of variations in the net charge on the dust grain in the present study is not sufficiently large to reach the possible saturation of the wake properties predicted by some studies [39].

The observed weak and stationary potential enhancements are consistent with previous simulations [18,19]. Such potential enhancements behind the dust grain can attract other dust grains and lead to the formation of vertical chains, which were observed in experimental devices [3,40]. We note here again that we expect this enhancement to be stronger in a three dimensional analysis. Our simulations were 25 times longer than previous molecular dynamics simulations, but we did not observe oscillating wake fields associated with the ion acoustic wake [9,10], seemingly because the linear response analysis is not appropriate in our case.

For supersonic velocities we observe the development of a Mach cone in potential as well as in electron and ion densities. For strong ion focusing we find that the focal region may trigger another perturbation so that the ion focus can serve as a source for a secondary Mach cone. Consequently, we can observe two cones behind an insulating object (see Fig. 13). For conductors, the ion focusing is usually too weak to be the source for a secondary cone. The focal region is less concentrated in this case.

The ions streaming out from the focal region have a significant velocity component perpendicular to the average drift, as seen from Fig. 3. The ion flow with a perpendicular velocity component has been mentioned as a possible explanation for the stationary off-axis alignment of a dust grain in the wake of the other dust, when the separation between grains is large enough [5]. Here, we refer to the axis as the line going through the first grain in the direction of the average ion drift. The dust grains used in the experiments [5] were made of melamine, and thus the analysis for the insulating obstacle is relevant here. The streaming ions lead to enhanced ion density and potential regions that are located off axis (see Figs. 4 and 13). This, together with the net momentum transfer due to ion-dust collisions, could act to keep the second dust grain slightly off axis when it is located in the wake of the first grain further down from the ion focus. For a negatively charged second dust grain, the resulting potential would have two stable extrema off axis, and the unstable extremum directly behind the first grain.

If we analyze particles with irregular surfaces (as in a previous study [23]), we observe irregular charge distributions on the surface. The surrounding electric field will give rise to a net torque on the particle, which will begin to rotate in the flow. Conservation of momentum is obtained when both the dust-grain and the plasma particles are taken into account. When the particle turns, it will also change the surface distribution of charge. Because of the large inertia of the dust particles, the short time duration of our simulations prohibits a detailed analysis of this process, which will be discussed in a different context. For the idealized symmetric dust grains studied in the present work, this phenomenon is not present. In reality, a small angular rotation can be expected even for strictly symmetrical bodies, because the surface charge distribution has a random component, which can be unsymmetrical (see, for instance, Fig. 15).

To summarize, there is a significant difference in the ion focusing behind the insulating and conducting grains of finite size that reflects the differences in the local charge density on the rear of the grain. In general, the ion focusing is stronger for colder ions, and will result in a locally enhanced potential behind the grain. The finite size effects and highly charged dust break the basic assumptions of the linear response theory. Therefore, one should be cautious when comparing the observations summarized here with potential or plasma density variations predicted by linear response theory, as applied for pointlike objects in other related studies [8–10,14].

ACKNOWLEDGMENTS

This work was supported in part by the Norwegian Research Council, NFR.

[1] P. K. Shukla and A. A. Mamun, *Introduction to Dusty Plasmas* (Institute of Physics Publishing, Bristol, Philadelphia, 2002).
[2] K. R. Svencs and J. Trøim, Planet. Space Sci. **42**, 81 (1994).
[3] A. Melzer, V. A. Schweigert, I. V. Schweigert, A. Homann, S. Peters, and A. Piel, Phys. Rev. E **54**, R46 (1996).
[4] K. Takahashi, T. Oishi, K.-I. Shimomai, Y. Hayashi, and S. Nishino, Phys. Rev. E **58**, 7805 (1998).
[5] G. A. Hebner and M. E. Riley, Phys. Rev. E **69**, 026405 (2004).
[6] V. A. Schweigert, I. V. Schweigert, A. Melzer, A. Homann, and A. Piel, Phys. Rev. E **54**, 4155 (1996).
[7] S. V. Vladimirov and M. Nambu, Phys. Rev. E **52**, R2172 (1995).
[8] M. Nambu, S. V. Vladimirov, and P. K. Shukla, Phys. Lett. A **203**, 40 (1995).
[9] O. Ishihara and S. V. Vladimirov, Phys. Plasmas **4**, 69 (1997).
[10] M. Lampe, G. Joyce, and G. Ganguli, Phys. Plasmas **7**, 3851 (2000).
[11] D. S. Lemons, M. S. Murillo, W. Daughton, and D. Winske, Phys. Plasmas **7**, 2306 (2000).
[12] L. J. Hou, Y. N. Wang, and Z. L. Mišković, Phys. Rev. E **64**, 046406 (2001).
[13] O. Ishihara, S. V. Vladimirov, and N. F. Cramer, Phys. Rev. E **61**, 7246 (2000).
[14] G. Lapenta, Phys. Rev. E **62**, 1175 (2000).
[15] I. H. Hutchinson, Plasma Phys. Controlled Fusion **47**, 71 (2005).
[16] G. Lapenta, Phys. Scr. **64**, 599 (2001).
[17] G. Lapenta, Phys. Rev. E **66**, 026409 (2002).
[18] F. Melandsø and J. Goree, Phys. Rev. E **52**, 5312 (1995).
[19] S. A. Maiorov, S. V. Vladimirov, and N. F. Cramer, Phys. Rev. E **63**, 017401 (2000).
[20] D. Winske, W. Daughton, D. S. Lemons, and M. S. Murillo, Phys. Plasmas **7**, 2320 (2000).
[21] I. V. Schweigert, V. A. Schweigert, and F. M. Peeters, Phys. Plasmas **12**, 113501 (2005).
[22] I. H. Hutchinson, Plasma Phys. Controlled Fusion **45**, 1477 (2003).
[23] W. J. Miloch, H. L. Pécseli, and J. Trulsen, Nonlinear Processes Geophys. **14**, 587 (2007).
[24] J.-P. Lafon, P. Lamy, and J. Millet, Astron. Astrophys. **95**, 295 (1981).
[25] A. V. Ivlev, G. Morfill, and V. E. Fortov, Phys. Plasmas **6**, 1415 (1999).
[26] J. W. Manweiler, T. P. Armstrong, and T. E. Cravens, J. Plasma Phys. **63**, 269 (2000).
[27] G. Lapenta, Phys. Plasmas **6**, 1442 (1999).
[28] S. V. Vladimirov, S. A. Maiorov, and N. F. Cramer, Phys. Rev. E **67**, 016407 (2003).
[29] S. V. Vladimirov, S. A. Maiorov, and O. Ishihara, Phys. Plasmas **10**, 3067 (2003).
[30] C. K. Birdsall and A. B. Langdon, *Plasma Physics via Computer Simulation* (Adam Hilger, Bristol, 1991).
[31] P. Guio and H. L. Pécseli, Phys. Plasmas **10**, 2667 (2003).
[32] F. Taccogna, S. Longo, and M. Capitelli, Contrib. Plasma Phys. **44**, 594 (2004).
[33] S. Teodoru, D. Tskhakaya, Jr., S. Kuhn, D. D. Tskhakaya, Sr., R. Schrittwieser, C. Ioniță, and G. Popa, J. Nucl. Mater. **337-339**, 1111 (2005).
[34] W. J. Weber, R. J. Armstrong, and J. Trulsen, J. Appl. Phys. **50**, 4545 (1979).
[35] A. Skøelv, R. J. Armstrong, and J. Trulsen, Phys. Fluids **27**, 2744 (1984).
[36] R. J. Armstrong, K. B. Liland, and J. Trulsen, Physica D **60**, 160 (1992).
[37] A. A. Samarian and B. W. James, Phys. Lett. A **287**, 125 (2001).
[38] L. Schott, in *Plasma Diagnostics*, edited by W. Lochte-Holtgreven (North Holland Publishing Company, Amsterdam, 1968), pp. 668–731.
[39] D. Winske, IEEE Trans. Plasma Sci. **29**, 191 (2001).
[40] V. Steinberg, R. Sütterlin, A. V. Ivlev, and G. Morfill, Phys. Rev. Lett. **86**, 4540 (2001).